Turbulent channel with slip boundaries as a benchmark for subgrid-scale models in LES

By A. Lozano-Durán AND H. J. Bae

1. Motivation and objectives

Most turbulent flows cannot be calculated by direct numerical simulation (DNS) of the Navier-Stokes equations because the range of scales of motion is so large that the computational cost becomes prohibitive. In large-eddy simulations (LES), only the large eddies are resolved and the effect of the small scales on the larger ones is supplied through a subgrid-scale (SGS) model in order to overcome most of the computational cost. In this sense, the role of SGS models is to provide the missing large-scale Reynolds stresses that can not be resolved in coarser LES computational grids.

Given that accurate representation of turbulence and prediction of flow behavior are needed in almost all engineering and scientific applications, validation of SGS models must be considered a task of paramount importance. Common reference solutions for LES validation are simple hydrodynamic cases such as forced or decaying isotropic turbulence (Métais & Lesieur 1992), spatial or temporal mixing layers (Vreman *et al.* 1996, 1997) and plane turbulent channel flow (Germano *et al.* 1991), among others. See Bonnet *et al.* (1998) for an overview of LES validation.

Most models explicitly or implicitly assume that the effective filter cutoff of the simulation lies within the inertial range, that is, far from the viscous effects but fine enough to represent the large-scale motions. This provides certain degree of universality to the flow and makes the modeling process more approachable. Hence, in order to properly evaluate a SGS model, the Reynolds number needs to be sufficiently large so the above conditions are reasonably well satisfied.

In test cases without walls, like isotropic turbulence, LES can be computed at relatively coarse grid resolutions while still meeting the aforementioned conditions. However, this requirement is impossible to fulfill in the near-wall region of wall-bounded flows such as turbulent channels or boundary layers, where the flow is dominated by the small viscous scales. The root of the problem lies at the formation of thin viscous layers required to force the no-slip boundary condition. As a result, the viscous stress is the dominant term in the momentum balance equation and the near-wall physics scale in wall units defined in terms of the kinematic viscosity and friction velocity at the wall. Therefore, in wall-bounded simulations where the resolution close to the wall is not fine enough, the SGS model must also supply the corresponding viscous stress, that is not the usual way they are designed to work.

The consequence is that most LES channel flows are wall-resolved and their Reynolds numbers are relatively low in order to reduce the computational cost of solving the near-wall region whose grid resolution requirements are not that far from DNS (Choi & Moin 2012). A possible solution is to incorporate wall-models that act as a surrogate of the near-wall dynamics, although this adds an extra modeling component that is intimately coupled with the SGS model under study and complicates the analysis.

In this brief, we present and discuss a new benchmark case to assess the performance

of SGS models in wall-bounded flows at high Reynolds numbers. The test mimics the physics of wall-bounded flows, as in turbulent channels, but without the necessity of either solving or modeling the near-wall region. The approach consists of a channel flow where the no-slip condition is replaced by a slip in the three velocity components that reduces the formation of near-wall viscous layers.

The paper is organized as follows. The formulation and proof of concept in DNS are presented in Section 2. An application to evaluate the performance of the dynamic Smagorinsky model is included in Section 3. Finally, we close the brief with conclusions.

2. Channel flow with a slip boundary condition

2.1. *Formulation*

We will consider first the incompressible Navier-Stokes equations in a rotating turbulent channel flow. The equations of motion are

$$\frac{\partial u_i}{\partial t} + \frac{\partial u_i u_j}{\partial x_j} = -\frac{1}{\rho}\frac{\partial p}{\partial x_i} + \frac{\partial}{\partial x_j}\left(\nu \frac{\partial u_i}{\partial x_j}\right) + 2\epsilon_{ijk} u_j \Omega_k, \quad \frac{\partial u_i}{\partial x_i} = 0, \tag{2.1}$$

where u_i, $i = 1, 2, 3$ are the streamwise, wall-normal and spanwise velocities, respectively, p is the pressure, ρ is the flow density, ν is the kinematic viscosity, ϵ_{ijk} is the Levi-Civita operator, and Ω_i is the rotational velocity. The three spatial directions are x_i, $i = 1, 2, 3$ and the walls are located at $x_2 = 0$ and $x_2 = 2h$ with h is the channel half-height. In the present study, we will consider only spanwise rotation, and the components of the rotation vector are given by $\Omega_3 = \Omega$. The centrifugal acceleration is absorbed into the pressure, and the last term of Eq. (2.1) represents the Coriolis force. See Grundestam *et al.* (2008) for details.

No-slip boundary conditions are applied at the walls

$$u_i = 0, \quad i = 1, 2, 3, \tag{2.2}$$

and the mean integrated streamwise momentum balance taking into account Eq. (2.2) is

$$\left\langle \nu \frac{\partial u_1}{\partial x_2} \right\rangle \Big|_{2h} - \left\langle \nu \frac{\partial u_1}{\partial x_2} \right\rangle \Big|_{0} = 2h \left\langle \frac{1}{\rho}\frac{\partial p}{\partial x_1} \right\rangle = 2u_\tau^2, \tag{2.3}$$

where $\langle \cdot \rangle$ denotes average in the homogeneous directions and time, and u_τ is the friction velocity. The friction Reynolds number is defined as $\mathrm{Re}_\tau = u_\tau h/\nu$. Equation (2.3) shows that the mean pressure gradient must be balanced by the viscous stress at the wall, and this is the mechanism responsible for generating thin viscous layers. The wall-normal thickness of this layer can be represented by high values of the mean viscous stress in the x_2 direction as shown for turbulent channel data and four Reynolds numbers in Figure 1. As Re_τ increases, the viscous layer becomes thinner in outer units. When re-scaled in wall units, denoted by the superscript $+$, the plots collapse and the thickness becomes constant in viscous units as shown in Figure 1(b).

To alleviate the formation of viscous layers we propose to replace the no-slip condition at the wall by a slip in the three velocity components of the form

$$u_i = l \frac{\partial u_i}{\partial x_2}, \quad i = 1, 2, 3, \tag{2.4}$$

where l is the slip length and the velocities u_i are, in general, non-zero at the wall. The

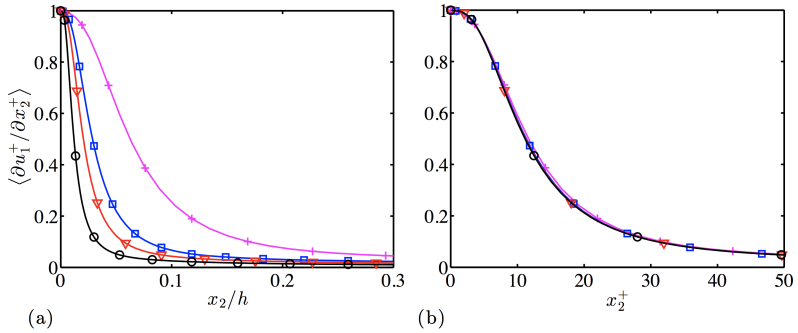

FIGURE 1. Mean viscous stress as a function of the wall-normal direction x_2 in (a) outer units and (b) wall units for four different Reynolds numbers in a turbulent channel flow. Symbols are equal to Re_τ as follows: +, 180; □, 395; ▽, 546; ○, 932. Data from del Álamo *et al.* (2004) and Lozano-Durán & Jiménez (2014).

equivalent to Eq. (2.3) is now

$$-\langle u_1 u_2 \rangle\Big|_{2h} + \langle u_1 u_2 \rangle\Big|_{0} + \left\langle \nu \frac{\partial u_1}{\partial x_2} \right\rangle\Big|_{2h} - \left\langle \nu \frac{\partial u_1}{\partial x_2} \right\rangle\Big|_{0} = 2h \left\langle \frac{1}{\rho} \frac{\partial p}{\partial x_1} \right\rangle = 2u_\tau^2. \tag{2.5}$$

The main difference between Eq. (2.3) and (2.5) is the extra tangential Reynolds stresses in the latter, and these are precisely the terms in charge of diminishing the emergence of viscous layers at the wall by balancing most of the mean pressure gradient. The effectiveness of Eq. (2.4) in achieving this goal will be discussed in Section 2.2.

Note that the dynamic system consisting of Eq. (2.1) with boundary conditions in Eq. (2.4) is well defined and can be solved by DNS but does not represent a real physical scenario. This is not an important concern as our goal is to generate wall-bounded-like turbulence in the interior of the domain without viscous layers even at the expense of non-physical boundary conditions.

Also note that although the present formulation includes a spanwise rotation of the channel, the non-rotating cases are equally valid and will serve the same purpose. Rotating cases will contain higher amount of energy in the large scales, which is less challenging for SGS models. Still, the symmetry in the x_2 direction with respect to the channel centerline is lost and even for moderate rotations the flow closer to the so-called stable wall adopts a laminar-like state, while the rest remains turbulent (unstable side). Such a transition from laminar to turbulent regime in the wall-normal direction is not trivial and must be correctly captured by the model.

In addition to LES applications, the channel flow with a slip is also an interesting testing case for understanding the underlying physics in the logarithmic layer (Marusic *et al.* 2013) when no rotation is applied. The attached-eddy hypothesis (Townsend 1961) assumes a self-similar hierarchy of eddies attached to the wall that follows from the fact that at a given x_2, the only meaningful physical quantities are u_τ and the distance to the wall. The only way eddies can feel the distance to the wall is through the boundary condition $u_2 = 0$, but the slip condition provides non-zero vertical velocity at the wall, challenging the fundamental premise of the attached-eddy model. Comparing the eddy structure in no-slip and slip channels may improve our knowledge about the role played by the wall in wall-bounded turbulence. However, this study is beyond the scope of the present paper and will be deferred to future investigations.

2.2. *Proof of concept in DNS*

We perform two DNS of rotating channel flow with slip boundaries at $\mathrm{Re}_\tau = 180$ and 395. The Rossby number for both cases is $Ro_\tau = 2\Omega h/u_\tau = 10$. The length, height and width of the computational domain are $2\pi h$, $2h$ and πh, respectively, and the simulations are driven by a constant pressure gradient. The streamwise and spanwise grid resolutions in wall units are uniform and equal to 9.7 and 4.8. A hyperbolic tangent was used to define the grid points in the wall-normal direction with a minimum and maximum grid spacing of 0.5 and 8.2 wall units. Both cases were run for 50 eddy turnover times after transients.

The value of l is arbitrary but must be set in outer units and independent of Re_τ to be consistent with our goal, e.g., by choosing a value equal to a constant fraction of the channel half-height h. After some preliminary studies, the slip length was chosen to be $l = 0.1h$. The particular choice of l is not relevant and the conclusions below are robust for different values. The only important constraint observed is that for a given Re_τ, the slip length must be larger than the thickness of the buffer layer. Taking the usual definition of 100 wall units, the buffer layer thicknesses for the two cases under consideration are $0.55h$ and $0.25h$, respectively, and the condition is satisfied when compared with $l = 0.1h$

The solutions are computed by integrating the incompressible Navier-Stokes equations with staggered second-order central finite-differences approximations as in Orlandi (2000). Time advancement is achieved by a third-order Runge-Kutta scheme (Wray 1990), combined with the fractional-step procedure (Kim & Moin 1985).

As an example, Figure 2 shows the instantaneous streamwise, wall-normal and spanwise velocities in a x_1–x_2 plane.

2.3. *One-point statistics*

Figure 3 shows the mean total and viscous stress as a function of the wall-normal direction. The former (Figure 3(a)) is defined as

$$\tau_{total} = -\langle u_1 u_2 \rangle + \left\langle \nu \frac{\partial u_1}{\partial x_2} \right\rangle, \tag{2.6}$$

and must follow the straight line

$$\tau_{total} = \frac{u_\tau^2}{h} y - \langle u_1 u_2 \rangle|_0 + \left\langle \nu \frac{\partial u_1}{\partial x_2} \right\rangle \Bigg|_0, \tag{2.7}$$

as imposed by the conservation of mean streamwise momentum. One of the contributors to τ_{total} is the viscous stress in Figure 3(b), which correspond to the second term in the right-hand side of Eq. (2.6). This last figure is of particular importance since it demonstrates that the viscous stress contribution at the turbulent unstable wall is less than 20% and 13% for $\mathrm{Re}_\tau = 180$ and 395, respectively, and that the trend is to decrease with increasing Reynolds numbers. This last observation aligns with the effect we were looking for, and SGS models are now free of the burden imposed by the previously dominant viscous stresses. Additionally, the grid point requirements close to the boundaries for LES applications do not scale in wall units anymore.

The mean profile and root-mean-squared (rms) velocity fluctuations are plotted in Figure 4. The reader should focus only on the solid lines, that correspond to the DNS data. We will not discuss the physical implications of these results but just stress that the profiles resemble those obtained in rotating channels with no-slip at the wall. This includes a linear region in the mean velocity profile with slopes close to twice the system

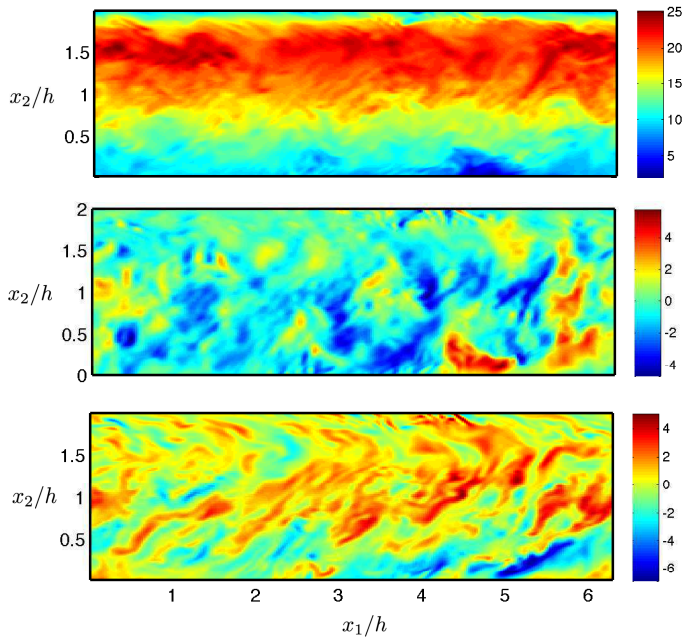

FIGURE 2. Instantaneous x_1–x_2 plane of the streamwise (top), wall-normal (center) and spanwise (bottom) velocities in a spanwise rotating channel flow with slip boundary conditions at the walls for $\mathrm{Re}_\tau = 395$ and $Ro_\tau = 10$. The colorbar shows velocity in wall units.

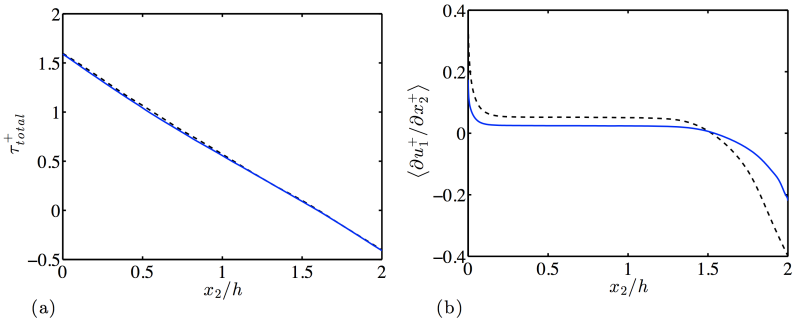

FIGURE 3. (a) Mean total and (b) viscous stress as a function of the wall-normal direction. Lines are dashed for $\mathrm{Re}_\tau = 180$ and solid for 395. The results shown are for DNS data.

rotation Ω, and an overall damping effect on the rms fluctuating velocities in the stable side (Grundestam *et al.* 2008).

3. Channel flow with slip as a benchmark for SGS models

In this section, we use the numerical experiment presented above as a benchmark for SGS models. LES calculations were carried out with the same code described in Section 2 with the dynamic Smagorinsky SGS model as in Germano *et al.* (1991) and Lilly (1991).

LES results are shown in Figure 4 (represented by symbols). The SGS model performs reasonable well and many features of the flow are correctly captured, including the typical

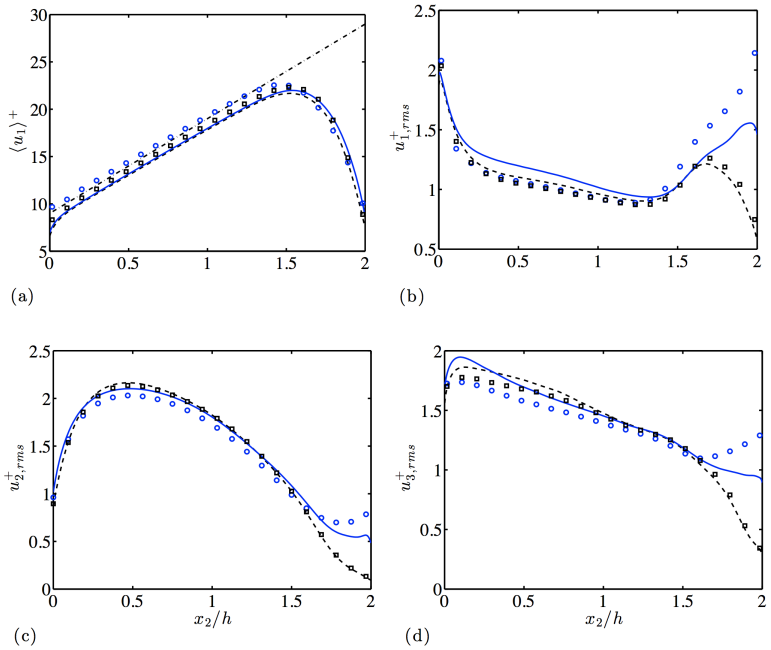

FIGURE 4. (a) Mean streamwise velocity profile. (b) Streamwise, (c) wall-normal and (d) spanwise rms velocity fluctuations. Lines are DNS at $\mathrm{Re}_\tau = 180$ (dashed) and 395 (solid). Symbols are LES at $\mathrm{Re}_\tau = 180$ (□) and 395 (○). The dash-dotted line in (a) has the slope 2Ω.

2Ω slope of the mean velocity profile and the peak locations of the rms fluctuations. However, there is a performance degradation with increasing Reynolds number, especially on the stable side, and it is unclear whether the trend will continue at more realistic higher Re_τ.

As discussed at the beginning of the brief, benchmarking should be done at high-Reynolds-number turbulence in order to faithfully evaluate the performance of SGS models. This is clearly not the case for the modest Reynolds numbers presented here and the results must be understood as a proof of concept. Future work will be devoted to the generation of reference high-Reynolds-number data required to test different SGS models in limiting cases.

4. Conclusions and future work

Validation and evaluation of the performance of SGS models is mandatory in LES. However, the formation of near-wall viscous layers in wall-bounded turbulence, especially at high Reynolds numbers, makes this task difficult.

In the present work, we have proposed a new benchmark case consisting of a turbulent channel flow where the no-slip condition at the wall was replaced by a slip in the three velocity components that suppresses the formation of near-wall viscous layers. We have shown that even at moderately low-Reynolds-numbers, these layers are reduced and the contribution of the viscous stress at the wall is smaller than 20%, and is expected to decrease for increasing Reynolds numbers. One-point statistics far from the wall are similar to those observed with the no-slip condition, making the present setup a suitable

test scenario for SGS models at high Reynolds numbers in a wall-bounded-like turbulent environment.

The results in this brief are a proof of concept and future work will focus on the generation of reference high-Reynolds-number data in channel flows with the slip boundary condition to challenge SGS models in controlled scenarios.

Acknowledgments

This work was supported by NASA under the Transformative Aeronautics Concepts Program, Grant #NNX15AU93A. The authors would like to thank Prof. Roel Verstappen for his discussions about the necessity of new benchmarks for SGS models that initiated the present work.

REFERENCES

Bonnet, J., Moser, R. & Rodi, W. 1998 *Selection of test cases for the validation of large eddy simulations of turbulent flows.* AGARD Advisory Report #345, Ch. 6.3 Jets, p. 35.

Choi, H. & Moin, P. 2012 Grid-point requirements for large eddy simulation: Chapman's estimates revisited. *Phys. Fluids* **24**, 011702.

del Álamo, J. C., Jiménez, J., Zandonade, P. & Moser, R. D. 2004 Scaling of the energy spectra of turbulent channels. *J. Fluid Mech.* **500**, 135–144.

Germano, M., Piomelli, U., Moin, P. & Cabot, W. H. 1991 A dynamic subgrid-scale eddy viscosity model. *Phys. Fluids* **3**, 1760.

Grundestam, O., Wallin, S. & Johansson, A. V. 2008 Direct numerical simulations of rotating turbulent channel flow. *J. Fluid Mech.* **598**, 177–199.

Kim, J. & Moin, P. 1985 Application of a fractional-step method to incompressible Navier-Stokes methods. *J. Comput. Phys.* **59**, 308–323.

Lilly, D. K. 1991 A proposed modification of the Germano subgrid-scale closure method. *Phys. Fluids*, **4** (3), 633–635.

Lozano-Durán, A. & Jiménez, J. 2014 Effect of the computational domain on direct simulations of turbulent channels up to $\mathrm{Re}_\tau = 4200$. *Phys. Fluids* **26**, 011702.

Marusic,I., Monty, J. P., Hultmark,M. & Smits,A. J. 2013 On the logarithmic region in wall turbulence. *J. Fluid Mech.* **716**, R3.

Métais, O. & Lesieur, M. 1992 Spectral large-eddy simulation of isotropic and stably stratified turbulence. *J. Fluid Mech.* **239**, 157–194.

Meyers, J. & Sagaut, P. 2007 Is plane-channel flow a friendly case for the testing of large-eddy simulation subgrid-scale models? *Phys. Fluids* **19**, 048105.

Orlandi, P. 2000 *Fluid Flow Phenomena: A Numerical Toolkit.* Kluwer.

Townsend, A. A. 1961 Equilibrium layers and wall turbulence *J. Fluid Mech.* **11**, 97–120.

Vreman, B., Geurts, B. & Kuerten, H. 1996 Large-eddy simulation of the temporal mixing layer using the Clark model. *Theor. Comp. Fluid Dyn.* **8**, 309–324.

Vreman, B., Geurts, B. & Kuerten, H. 1997 Large-eddy simulation of the turbulent mixing layer. *J. Fluid Mech.* **8**, 357–390.

Wray, A. A. 1990 *Minimal-storage time advancement schemes for spectral methods.* NASA Tech. Rep. #MS 202 A-1.